International Journal of Automotive Technology, Vol. 22, No. 2, pp. 455–463 (2021)
DOI 10.1007/s12239–021–0042–2

pISSN 1229–9138/ eISSN 1976–3832

SOOT DEVELOPMENT IN AN OPTICAL DIRECT INJECTION SPARK IGNITION ENGINE FUELED WITH ISOOCTANE

Fangxi Xie[1,2], Miaomiao Zhang[3], Yongzhen Wang[1,2], Yan Su[1,2]*, Wei Hong[1,2] and Peng Cheng[1,2]

[1]State Key Laboratory of Automotive Simulation and Control, Jilin University, Changchun 130025, China
[2]College of Automotive Engineering, Jilin University, Changchun 130025, China
[3]School of Mechanical and Electrical Engineering, Jiangsu Normal University, Xuzhou 221116, China

(Received 26 December 2019; Revised 23 May 2020; Accepted 20 June 2020)

ABSTRACT–To better understand the formation and evolution processes of soot, the two-color laser induced incandescence diagnostic method was applied on a single cylinder optical direct injection spark ignition engine. Soot volume fraction was measured, and soot distribution was imaged as cyclic fuel quantity changes. The results show that 45.5 mg/cycle generates the most soot at the same measure plane. Pool fire dominates the formation of soot in the tested engine and generates more soot on the top surface of the piston near the injector. In-cylinder soot increases until 42°CA ATDC and then reduces due to oxidation. Pool fire continues through the expansion stroke till 52°CA ATDC, and then soot cloud gathers near the 10 mm plane. After 82°CA ATDC, in-cylinder soot basically in equilibrium, and residual soot moves follow the in-cylinder flow randomly and evenly distributes within the whole combustion chamber. With increasing cyclic fuel quantity, particles number concentration gradually increases and their distribution present dual-peak shape. In detail, 45.5 mg/cycle emits the most accumulation mode particles while 52 mg/cycle emits the most nucleation mode particles.

KEY WORDS : Soot, Laser induced incandescence, 2-Colour, GDI engine, Particles

NOMENCLATURE

ATDC : after top dead center
BTDC : before top dead center
DISI : direct injection spark ignition (DISI)
GDI : gasoline direct injection (GDI)
ICCD : intensified charge coupled device
ICE : internal combustion engine
LEM : laser extinction method
LII : laser induced incandescence
2C-LII : 2 color-laser induced incandescence

1. INTRODUCTION

Owning to its efficiency, durability, low cost and high-power density, ICE (internal combustion engine) will remain the dominant power unit for moveable machines and systems within the next few decades (Niessner, 2014). Compared with other techniques for improving energy efficiency of ICEs, GDI (gasoline direct injection) may be more attractive for the automotive market in recent years (Costa *et al*., 2016). Despite the advantages, GDI engines also produce unavoidable fine and ultrafine particles due to the more likely happened local fuel-rich and wetting phenomenon in combustion chamber (Zimmerman *et al*., 2016; Zhang *et al*., 2018a; Seong *et al*., 2013). Modern society pays more attention to the reduction of engine particles because of its risk for human health. Thus, researches about the formation mechanism and reduction methods of engine particles need to be promoted for the purpose of achieving zero emission engines.

Compared with particles emitted from diesel engines, GDI engine particles show similar mixture formation mode and morphology (La Rocca *et al*., 2015; Uy *et al*., 2014). Therefore, the generally adapted formation mechanism of particles for GDI engines are based on and transferred from diesel engines (Kittelson, 1998). To sum up, the formation and development of particles can be described by six processes: pyrolysis, nucleation, surface growth, coalescence, agglomeration and oxidation (Amann and Siegla, 1981). Eventual engine out particles are a balance between formation and oxidation and own large range of size. Generally, engine particles are divided into two modes: the nucleation mode (diameter < 35 nm) which consist of volatile organic and sulfur compounds, and the accumulation mode (diameter > 35 nm) which consist of carbonaceous agglomerates (soot).

For GDI engines, combustion and particles formation processes depend critically on the mixture preparation, which exert a very substantial effect on the rate of fuel-air mixing and the degree of mixture stratification. Locally rich

*Corresponding author. e-mail: suyan@jlu.edu.cn

mixture burning, and pool fire are the two principal soot sources of direct-injection spark-ignition (DISI) engine (Stojkovic *et al*., 2005), while the latter is the prominent factor (Koegl *et al*., 2018). Several investigations have been performed to study combustion and soot processes of SIDI engines. Stevens and Steeper (2001) combined optical diagnostics to an optical DISI engine and revealed the close relationship between piston-top fuel film, pool fire and particles. They found that significant amounts of particles were produced by pool fire, which can burn until midway through the exhaust stroke. Anbari Attar and Xu (2016) investigated effects of fuel wetting and mixture preparation on particle emissions. The results revealed that fuel impingement on hot piston and consequent fuel pyrolysis and diffusion flame primarily produce accumulation mode particles, while late fuel wetting on cylinder liner primarily generate nucleation mode particles. Li *et al*. (2017) demonstrated the effect of cooled EGR on soot emission and found that lowered reaction temperature of pool fire is the primary contributor to reduce soot emission.

Optical diagnostics, as the in-situ measuring techniques, are widely used to examine combustion process and products within internal combustion engines. In terms of soot emissions, three main optical techniques have been applied traditionally: 2-colour pyrometry method (2C), laser extinction method (LEM) and laser induced incandescence (LII). In comparison with the other two line-of-sight methods, LII is able to measure soot distribution at any plane (Pastor *et al*., 2016), and has been successfully applied in studying soot formation and development processes in flames (Wang *et al*., 2018; Witkowski *et al*., 2013), constant volume vessels (Zheng *et al*., 2015) as well as in optical engines (Menkiel *et al*., 2014; Rao *et al*., 2018). Furthermore, combination of LII and 2C (Snelling *et al*., 2005) or LEM (de Francqueville *et al*., 2010) can still be used as quantitative measurement. As diesel engines account for the major amount of soot emissions from vehicles, LII techniques have always been used to research soot formation in compression ignition optical engines fueled with diesel (Lee *et al*., 2004; Bobba and Musculus, 2012; Menkiel *et al*., 2012), biodiesel (Su *et al*., 2018; Zhang *et al*., 2019) and diesel alternative fuels (Miles *et al*., 2007; Leermakers and Musculus, 2015) in the past few decades. However, with the increasingly applied technique of gasoline direct injection, LII is becoming more widely used in studying soot from optical direct injection spark ignition engines in recent years. de Francqueville *et al*. (2010) applied the coupled method of LII and LEM to perform quantitative measurement of soot inside a gasoline optical engine, and the hypothesis that soot formation is mostly conditioned by fuel-rich zones was supported. Velji *et al*. (2010) combined Rayleigh-scattering, LII and extinction techniques in an optical DISI engine. They found that in the homogeneous mode the main cause of soot formation are pool fires, while in the stratified mode local rich mixture regions together with pool fires play the dominant factors in the soot formation.

Limited number of literatures have preliminary revealed the formation mechanism of soot in GDI engines, while the soot distribution and soot evolution of the entire combustion chamber need more in-depth research. The current paper first established a 2C-LII quantitative measurement platform. And then, this laser diagnostic method was applied in an optical DISI engine fueled with isooctane to measure in-cylinder soot volume fraction and to research soot distribution as the mixture concentration changes and soot development in the entire combustion chamber. This paper provides a much more detailed description of soot distribution and soot development, and clearly reveals the key factor that affect soot formation in DISI engine. It is conducive to the understanding of in-cylinder soot formation mechanisms, and to the controlling of engine out soot emissions. It will also provide quantitative references and validation for the optimization of combustion model.

2. EXPERIMENTAL SETUP AND DIAGNOSTICS

2.1. Theory of 2C-LII Methods

Assuming that soot particles were heated uniformly to the same temperature because of the spatially uniform fluence of laser sheet, one can calculated soot temperature T_P by two-color pyrometry method (Snelling *et al*., 2005) as follows

$$T_P = \frac{\frac{hc}{k}\left(\frac{1}{\lambda_{C_1}} - \frac{1}{\lambda_{C_2}}\right)}{\ln\left(\frac{I_{EXP_1}\eta_2\lambda_{C_1}^6 E(m_{\lambda_1})}{I_{EXP_2}\eta_1\lambda_{C_2}^6 E(m_{\lambda_2})}\right)}$$

where h is the Planck constant, c is the speed of light, k is the Boltzmann constant, λ_{C_1} and λ_{C_2} are the two center wavelengths, I_{EXP1} and I_{EXP2} are the voltage signal of ICCD camera corresponding to two wavelengths, $E(m_\lambda)$ is the soot absorption function (a constant value of 0.26 was chose in this paper according to reference (Snelling *et al*., 2005) and (Smallwood *et al*., 2002).

Soot volume fraction is given by

$$f_v = \frac{I_{EXP}}{\eta\omega_b\frac{12\pi c^2 h}{\lambda_C^6}E(m_\lambda)\left[exp\left(\frac{hc}{k\lambda_C T_P} - 1\right)\right]^{-1}}$$

where ω_b is the thickness of laser sheet, η is a defined factor that can be written as

$$\eta = GM^2 A_P \frac{A_L}{u^2}\Theta(\lambda_C)\Delta f\tau(\lambda_C)$$

where G is the amplification multiple, M^2A_P is the area of measurement field that corresponds to one pixel, A_L is

the area of the aperture, A_L/u^2 is the collection solid angle of the lens, $\Theta(\lambda)$ is the voltage signal per watt, Δf is the bandwidth of the filter, $\tau(\lambda)$ is the filter transmission as a function of wavelength.

2.2. Laser Diagnostic Setup

Figure 1 shows the optical schematics for laser induced incandescence of this work. The laser diagnostic system used here consisted of a pulsed Nd: YAG laser (LOTIS LII, LS-2137M), a sheet and collimator optics, and an ICCD camera (La Vision, Imager Pro X 2M). The camera was fitted with a lens (Nikon PF10545MF-UV) and an image doubler fixed with two band-pass filters with their central wavelength at 400 nm (FWHM = 50 nm) and 600 nm (FWHM = 10 nm). The two central wavelengths were selected for higher accuracy of soot temperature and soot volume fraction (Liu *et al.,* 2009). In order to avoid the interference of fluorescence (polycyclic aromatic hydrocarbon and other species during combustion) and easily arrange the light pass, the laser operated at 532 nm with a pulse repetition rate of 10 Hz and a pulse width of 7 ns, and its output power was 170 mJ. The laser light was formed into a light sheet (1 × 66 mm) by the sheet and collimator optics and then introduced into the flame. The LII images were captured by the ICCD camera with a gate of 20 ns, a gain of 75 and a delay of 60 ns. These setups were determined to guarantee the instantaneity and adequacy of LII signals.

2.3. Engine Setup and Operation Conditions

The experiments were conducted in a single-cylinder optical direct injection spark ignition engine modified from a commercial 1.4-L, 4-cylinder GDI engine. The piston is extended, and a flat quartz piston crown is assembled on it, the diameter of the crown is 55 mm in top and 60 mm in bottom. In addition, a cylinder liner quartz window is located on the top of the cylinder wall, which not only provides sheet laser access horizontally but also makes vertically imaging diagnostic available. The inner and external diameter of the quartz liner is 80 mm and 120 mm, respectively, and the height is 50 mm. A 45 ° reflection mirror is fixed within the extended piston so that the in-cylinder horizontal image could be observed. The injector with 6 holes is located aside and the spark plug is centrally mounted. Two intake valves and two exhaust valves are equipped in this optical engine, and the entrance side of the sheet laser into the cylinder is near to the intake valve. More engine specifications are summarized in Table 1.

Table 1. Detailed optical engine specifications.

Engine Parameters	Specifications
Engine Type	Single-cylinder, 4-stroke, 4-valve
Bore	80 mm
Stroke	75.6 mm
Connecting rod length	135 mm
Compression ratio	8:1
Combustion system	Spray-Guided

The engine speed was fixed at 600 rpm by an alternating current dynamo throughout the optical engine experiments. An AVL quartz crystal pressure sensor with model of ZF42 was used to measure the combustion pressure in cylinder, and it was installed in the place of spark plug. An AVL

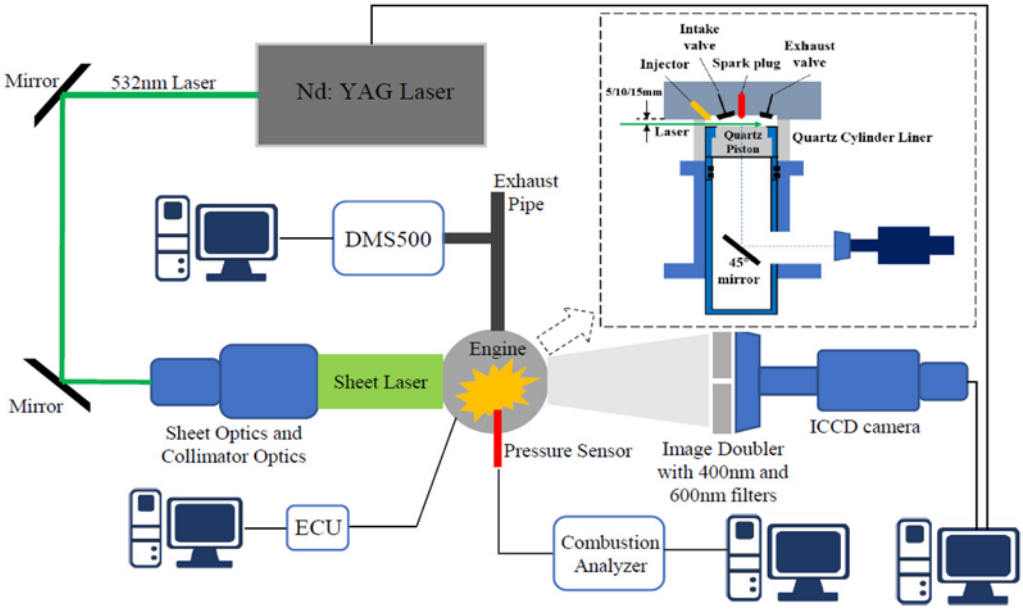

Figure 1. Optical setup for laser induced incandescence of optical engine fueled with isooctane.

charge amplifier was employed to process and amplify pressure signal, and a LF-72BMC05E encoder with 1 ° resolution was used to acquire the crankshaft angles. Combustion process was calculated by AVL 461 combustion analyzer. In the test, a self-developed electronic control (ECU) based on the 16-bit Freescale single-chip was employed to flexibly control the engine fuel injection pulse width, timing and pressure. The particle size distribution and particle number concentration were measured by a Combustion DMS500 Fast Particulate Analyzer, and its size spectrum is from 4.87 to 1000 nm, the data was recorded at a sampling frequency rate of 10 Hz.

In this paper, isooctane was used as fuel, the interference of fluorescence emitting from aromatic hydrocarbons in gasoline can be avoided. The injection pressure was 12 MPa, which is the highest pressure of the injection system. Injection timing and ignition timing, determined according to the original engine data, were held constant at 240°CA BTDC and 10°CA BTDC, respectively. The intake air charge mass flow was maintained at 9 kg/h. Three laser planes (5, 10, 15 mm below the cylinder head) were selected so that the spatial information of soot could be visualized. Three injection pulse width (6000, 7000, 8000μs) were used to compare the impacts of cyclic fuel quantity on soot characteristics. These three operating conditions can ensure a certain shooting effect, and at the same time make the corresponding peak cylinder pressure appear inflection point. Their corresponding fuel quantities were 39 mg/cycle, 45.5 mg/cycle and 52 mg/cycle respectively. At 52 mg/cycle condition of each plane, several reference times of laser and camera trigger were selected in order to visualize temporal soot development information. During the experiment, the engine operated in a consecutively-ignition and skip-injection mode, and the trigger of the optical diagnostic system was based on injection timing.

3. RESULTS AND DISCUSSION

The in-cylinder pressure values at different fuel quantities were shown in Figure 2. The engine was operated in skip-injection mode for the sake of the reduction of soot deposit on quartz liner and piston window. Due to this discontinuous operating condition, the excess air coefficient (λ) was unable to monitored steadily by lambda meter. Assuming the injected isooctane evaporated completely, according to the characteristics of the injection system, at this condition of intake flow, the excess air coefficients are 0.83, 0.74 and 0.64, respectively. However, because of the incomplete evaporation of fuel, which was attributed to the lower combustion chamber temperature, the values of real excess air coefficients for the in-cylinder mixture were higher. As clear from Figure 2, the peak in-cylinder pressure of 45.5 mg/cycle was the highest, followed by 52 mg/cycle and then 39 mg/cycle. In light of the variation curve of thermal efficiency resulting from changing excess air ratio (Park *et al*., 2016; Bontorin and de Oliveira Carvalho, 2016), the actual excess air coefficient of 45.5 mg/cycle might be about 1.0 ~ 1.2. By that analogy, the actual mixture of 39 mg/cycle was leaner (λ > 1.2), and the 52 mg/cycle was thicker (λ < 1).

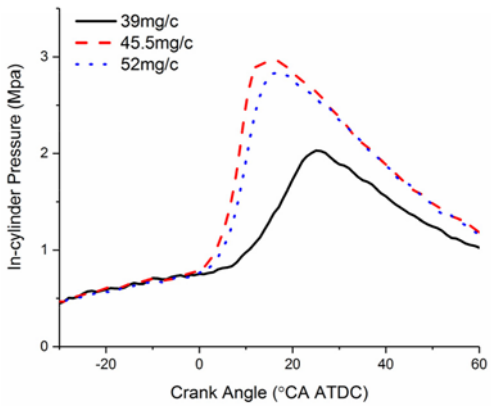

Figure 2. In-cylinder pressure at different fuel quantities.

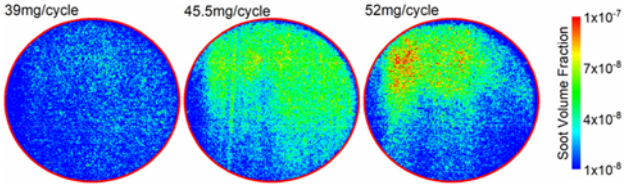

Figure 3. Distributions of soot for 5 mm plane at 32 °CA ATDC.

Figure 3 denotes the effects of fuel quantity on distribution of soot at 5 mm plane. The observation timing was 32°CA ATDC at which moment the laser could just flit across top of quartz piston for 5 mm plane. Each image is the averaged result of at least 10 individual images, and the red circle was added to indicate the combustion boundary of quartz liner. The laser was directed from top to bottom of each image, and the intake valves locate on the top side while the exhaust valves locate on the bottom side.

An overall uniform distribution of soot is detected for 39 mg/cycle and the peak and average soot volume fraction are both the lowest seen from Figure 4 (a). As increasing fuel quantity, nonuniformity became stronger and most of soot cluster on the top side where near the intake valves and injector. This trend of distribution was partially attributed to the attenuation of laser sheet, but most importantly, was due to the local rich regions when the mixture became thicker. In addition, piston impingement became serious when more fuel was injected for this spray-guided combustion chamber (Zhang *et al*., 2018b), so the top side of the piston, near the injector, became more wet, thus poor-fire occurred and more soot was generated. This can be demonstrated by the obvious piston-top carbon deposits after several fired cycles.

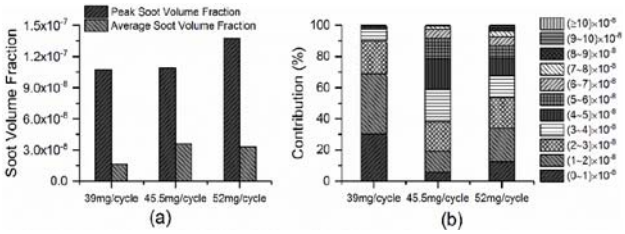

Figure 4. Soot volume fraction at 5 mm plane; (a) peak and average soot volume fraction, (b) contributions of each soot volume fraction range.

Also is shown in Figure 4 (a), the peak soot volume fraction gradually raises, while the average value of 52 mg/cycle is lower than that of 45.5 mg/cycle which reflects the more uneven distribution of soot for 52 mg/cycle. Presented in Figure 4 (b) is the contribution of each soot volume fraction range. At 39 mg/cycle, about 98 % of pixels have soot volume fraction in the range of $(0 \sim 4) \times 10^{-8}$ at the tested plan. When the mixture gets thicker, pixels with a large fraction value become much more and the nonuniformity is shown.

The development of soot for the 5 mm plane at 52 mg/cycle is shown in Figure 5. With the piston down, on the whole, the level of soot decreases, and the distribution became more uniform throughout the combustion chamber. Two main reasons were attributed to this phenomenon at the measured plane. The first one was that when the crank angle became larger at the expansion stroke, the volume of mixture increased, thus the looser soot made a low level of soot volume fraction. Also contributing, to some degree, are augments in time for liquid fuel to vaporize and for the initially formed soot to oxidize with air or some intermediate products. It can be seen from Figure 5 that at 72°CA ATDC, only sporadic and negligible amount of soot was detected at 5 mm plane. While for 82°CA and 92°CA ATDC, partial high soot volume fractions were observed which are mainly due to in-cylinder charge motion and random soot distribution within the combustion chamber. Another explanation may be that along with the dynamical flow, soot in the chamber gathered irregularly, thus the fluctuation happened.

For 10 mm plane, the distributions and soot volume fraction are shown in Figures 6 and 7 respectively. It is clear that at this measured plane, the peak and average soot volume fraction of 39 mg/cycle is the lowest, followed by 52 mg/cycle, and 45.5 mg/cycle is the highest. Like the 5 mm plane, nonuniformity becomes serious as increasing fuel quantity, and most of soot was detected on the top side of the visible range. Compared with 5 mm plane, 10 mm plane owns more soot. As mentioned above, impingement generated a lot of soot spatially near the top of piston. Although the amount of soot in the upper space was reduced

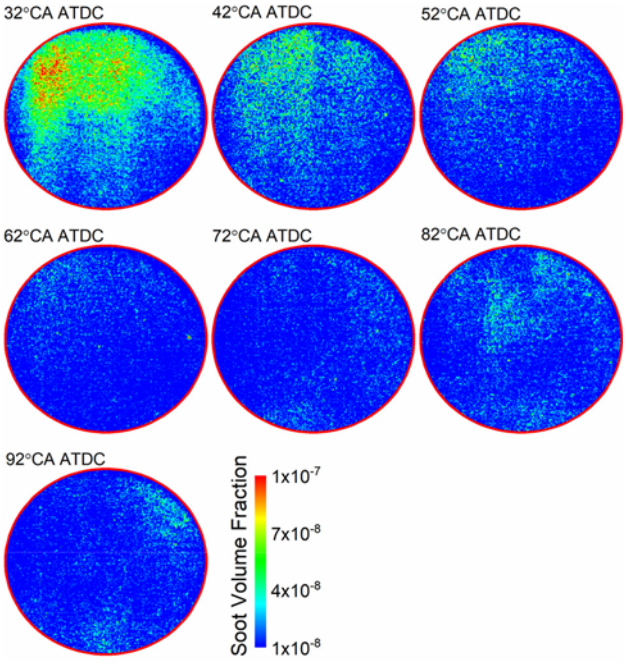

Figure 5. Development of soot for 5 mm plane at 52 mg/cycle.

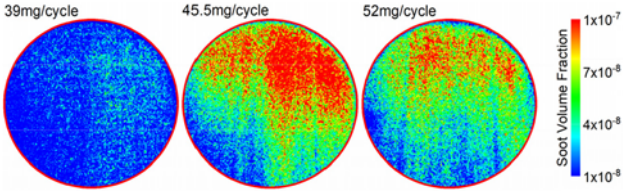

Figure 6. Distributions of soot for 10 mm plane at 42°CA ATDC.

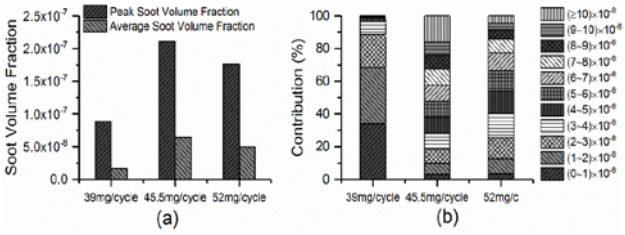

Figure 7. Soot volume fraction at 10 mm plane; (a) peak and average soot volume fraction, (b) contributions of each soot volume fraction range.

due to on-going oxidation, more fuel vaporized and then combusted rapidly because of the increased temperature during combustion. Also, it can be seen from the result that a decrease in soot was observed from 45.5 mg/cycle to 52 mg/cycle. Combustion temperature is a key factor that affects the formation of soot. For 52 mg/cycle, a relatively

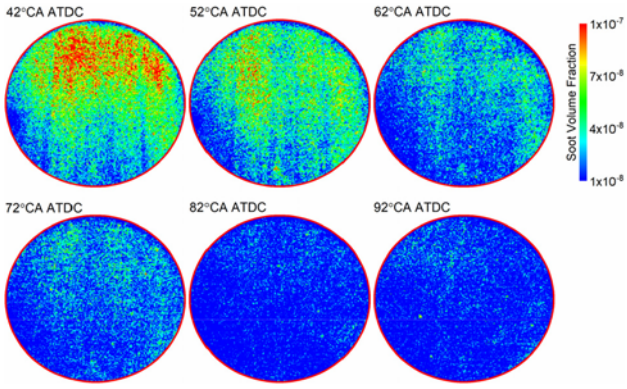

Figure 8. Development of soot for 10 mm plane at 52 mg/cycle.

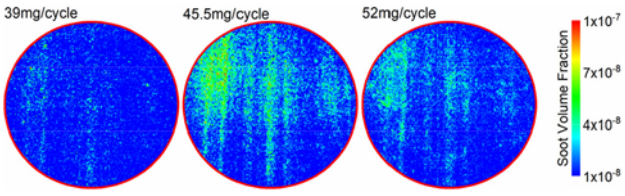

Figure 9. Distributions of soot for 15 mm plane at 52°CA ATDC.

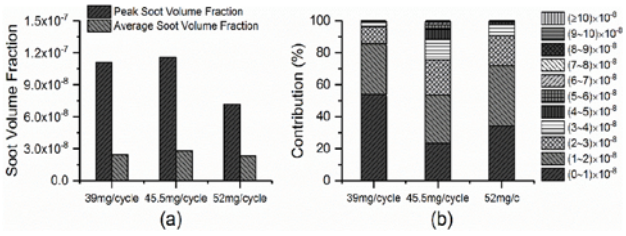

Figure 10. Soot volume fraction at 15 mm plane; (a) peak and average soot volume fraction, (b) contributions of each soot volume fraction range.

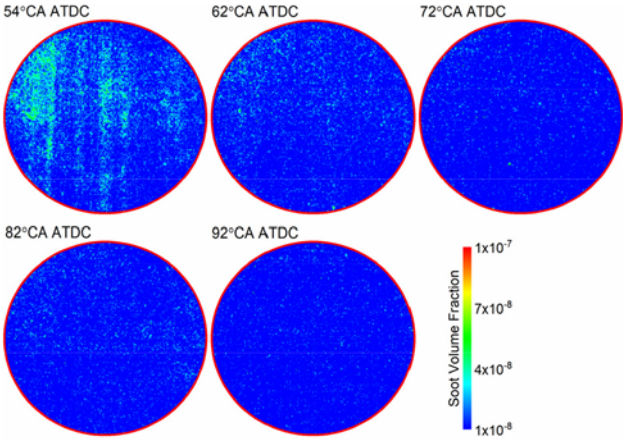

Figure 11. Development of soot for 15 mm plane at 52 mg/cycle.

lower excess air ratio made the fuel incompletely combusted, thus the in-cylinder combustion temperature was lower than 45.5 mg/cycle. As a result, the dehydrogenation reaction was suppressed, and the formation of primary carbonaceous particles was facilitated. Additionally, the pool-fire was more prominent due to longer injection duration and slower fuel evaporation. All these factors result in a lower peak and average soot volume fraction for 52 mg/cycle compared to that of 45.5 mg/cycle. Typically, pixels with soot volume fraction larger than 1×10^{-7} accounted for 16 percent of the whole detected area at 45.5 mg/cycle condition.

The development of soot for 10 mm plane is shown in Figure 8. With delay of the detect timing, the amount of soot reduced gradually at this measured plane and the distribution became more uniform throughout the combustion chamber. The reason for this change trend can be referred to the previous explanation at 5 mm plane. Seen from Figures 5 and 8, another conclusion could be made that the amount of soot for 10 mm plane is more than that of 5 mm plane at the same moment.

Soot characteristics of the 15 mm plane are depicted in Figures 9 to 11. Compared with the above results, the smallest amount of soot was detected on this plane. At this late combustion phase, no more soot was generated and the initially formed soot oxidized sufficiently with their level decreased. The peak and average soot volume fraction both increase first and then decrease as increasing cyclic fuel quantity. The reason can be explained by the same sayings as above (10 mm plane). Throughout the entire plane, points with soot volume fraction of $(0 \sim 4) \times10^{-8}$ contributes over 90 percent to all tested pixels. Similarly, seen from Figure 11, the amount of soot gradually reduced as the piston moved towards bottom dead center, and negligible soot was detected at 15 mm plane after 72°CA ATDC.

Figure 12 gives the variation of particles number concentration and particles size-number distribution when increasing fuel quantity. The nucleation mode represents particles in a small diameter range (0 ~ 30 mm), which usually consist of volatile organic that is attributed to condensation of hydrocarbon during exhaust dilution and cooling. The accumulation mode represents particles in a large diameter range (30 ~ 500 mm), which usually consist of soot agglomerates from local rich mixture in the combustion chamber (Burtscher, 2005). A rising trend was found in total particulate number concentration when richer mixture was combusted, while nucleation mode showed the opposite variation to accumulation mode. As discussed above, 45.5 mg/cycle condition formed the most amount of soot, which was the major constituent of accumulation mode particles. Therefore, there are more

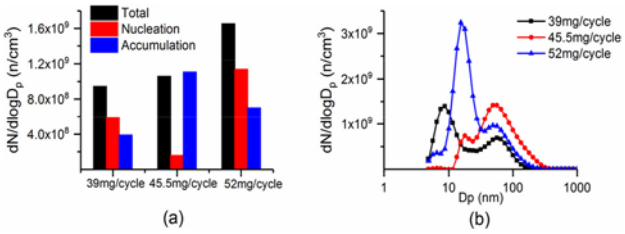

Figure 12. Particulate matter characteristics; (a) particulate number concentration, (b) particulate matter number-size distribution.

particles with large particle size in exhaust emissions. While for 52 mg/cycle, a large amount of fuel was incompletely combusted, the condensation and cooling of hydrocarbon was enhanced due to the increased THC emissions. Consequently, the nucleation mode of particles at 52 mg/cycle was higher than that of other conditions. It is also clear that all cases performed similar distribution with dual-peak, the first peak fell within 10~20 nm and the second peak fell within 60~80 nm. These two peaks correspond to the peak values of the particle concentration of the two modes, respectively. Typically, the sharp increase in the concentration of nucleation particles dominates the increase in total particle concentration under 52 mg/cycle condition.

The soot development process at 52 mg/cycle is displayed in Figure 13. The results revealed that pool fire was the primary contributor to the rising soot formation. During the expansion stroke process, soot in the entire combustion chamber increased to the most at 42°CA ATDC and then decreased gradually on account of the on-going soot oxidation. For the tested optical engine, sooting pool fire persist through the expansion stroke till 52°CA ATDC, and then soot cloud gathered near the 10 mm plane till 72°CA ATDC. After 82°CA ATDC, the soot oxidation was almost completed due to limited in-cylinder temperature and the remaining soot is homogeneously distributed throughout the whole cylinder.

4. CONCLUSIONS

The 2-color laser induced incandescence measuring system was used in this paper, effects of cyclic fuel quantity on soot volume fraction and soot distribution were researched in a single cylinder optical DISI engine fueled with isooctane, and an intuitive description of soot development was revealed through this work.

As the amount of fuel quantity increases, the average soot volume fraction of the measured plane increases first and then decreases, and the non-uniformity of soot distribution increases. Of the three plans studied, 45.5 mg/cycle generates the highest average soot volume fraction, and soot is gathered on the top surface of piston close to injector.

The amount of in-cylinder soot reaches the highest at about 42°CA ATDC and then reduces because of oxidation process. Pool fire dominates the formation of soot in the tested optical engine and lasts through the expansion stroke until 52°CA ATDC. Then soot clouds gather near the 10 mm plane. After 82°CA ATDC, in-cylinder soot basically reaches a balance status. Residual soot randomly moves follow the in-cylinder flow and almost evenly distributes within the combustion chamber.

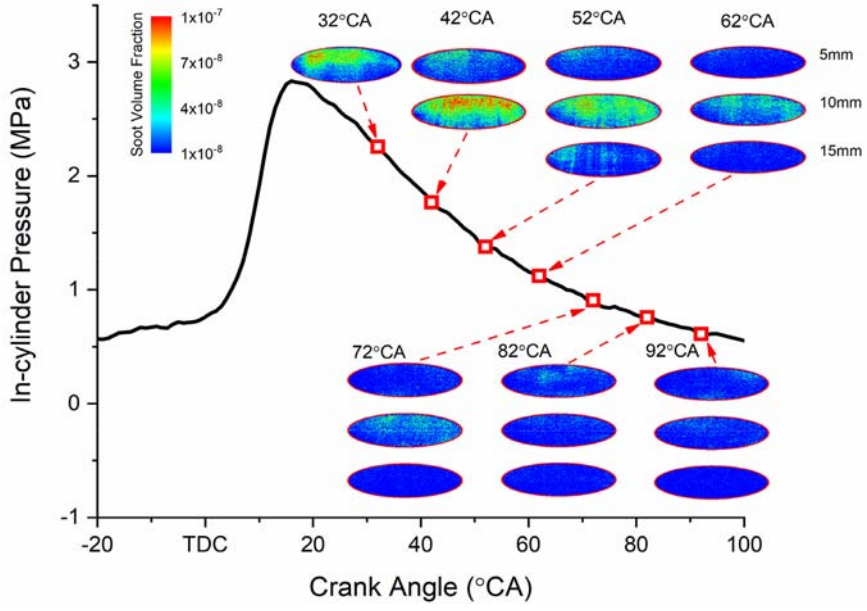

Figure 13. In-cylinder soot distribution and development at 52 mg/cycle.

The optically measured soot information is in good agreement with the particulate information measured from exhaust gas. With adding cyclic fuel quantity, particles number concentration gradually increases, while 45.5 mg/cycle emits the most accumulation mode particles and 52 mg/cycle emits the most nucleation mode particles.

ACKNOWLEDGEMENT–This work was financially supported by National Natural Science Foundation of China (Grant No. 51876079), Science and Technology Pilot Projects of Jilin Province (20180201008GX), Provincial Fund Projects of the Industrial Innovation of Jilin Province (2019C058-4), Science and Technology Pilot Projects of Jilin Province (20190103049JH), Open Fund of state key laboratory of automotive simulation and control, Jilin University (20181110), Science and Technology Research Projects of Jilin Province education department for 13th Five Year Plan (JJKH20200978KJ), the Fundamental Research Funds for the Central Universities.

REFERENCES

Amann, C. A. and Siegla, D. C. (1981). Diesel particulates —what they are and why. *Aerosol Science and Technology* **1**, **1**, 73–101.

Anbari Attar, M. and Xu, H. (2016). Correlations between particulate matter emissions and gasoline direct injection spray characteristics. *J. Aerosol Science*, **102**, 128–141.

Bobba, M. K. and Musculus, M. P. B. (2012). Laser diagnostics of soot precursors in a heavy-duty diesel engine at low-temperature combustion conditions. *Combustion and Flame* **159**, **2**, 832–843.

Bontorin, A. C. B. and de Oiveira Carvalho, L. (2016). Investigation of the Impact of Lean Mixtures on the Performance of GDI Engines. *SAE Paper No.* 2016-36-0326.

Burtscher, H. (2005). Physical characterization of particulate emissions from diesel engines: a review. *J. Aerosol Science* **36**, **7**, 896–932.

Costa, M., Catapano, F., Sementa, P., Sorge, U. and Vaglieco, B. M. (2016). Mixture preparation and combustion in a GDI engine under stoichiometric or lean charge: an experimental and numerical study on an optically accessible engine. *Applied Energy*, **180**, 86–103.

de Francqueville, L., Bruneaux, G. and Thirouard, B. (2010) Soot volume fraction measurements in a gasoline direct injection engine by combined laser induced incandescence and laser extinction method. *SAE Int. J. Engines* **3**, **1**, 163–182.

Kittelson, D. B. (1998). Engines and nanoparticles: a review. *J. Aerosol Science* **29**, **5-6**, 575–588.

Koegl, M., Hofbeck, B., Will, S. and Zigan, L. (2018). Investigation of soot formation and oxidation of ethanol and butanol fuel blends in a DISI engine at different exhaust gas recirculation rates. *Applied Energy*, **209**, 426–434.

La Rocca, A., Bonatesta, F., Fay, M. W. and Campanella, F. (2015). Characterisation of soot in oil from a gasoline direct injection engine using Transmission Electron Microscopy. *Tribology Int.*, **86**, 77–84.

Lee, K. H., Chung, J.W., Kim, B. S. and Kim, S. K. (2004). Investigation of soot formation in a DI diesel engine by using laser induced scattering and laser induced incandescence. *KSME Int. J.* **18**, **7**, 1169–1176.

Leermakers, C. A. J. and Musculus, M. P. B. (2015). In-cylinder soot precursor growth in a low-temperature combustion diesel engine: Laser-induced fluorescence of polycyclic aromatic hydrocarbons. *Proc. Combustion Institute* **35**, **3**, 3079–3086.

Li, T., Yin, T. and Wang, B. (2017). Anatomy of the cooled EGR effects on soot emission reduction in boosted spark-ignited direct-injection engines. *Applied Energy*, **190**, 43–56.

Liu, F., Snelling, D. R., Thomson, K. A. and Smallwood, G. J. (2009). Sensitivity and relative error analyses of soot temperature and volume fraction determined by two-color LII. *Applied Physics B* **96**, **4**, 623–636.

Menkiel, B., Donkerbroek, A., Uitz, R., Cracknell, R., and Ganippa, L. (2012). Measurement of in-cylinder soot particles and their distribution in an optical HSDI diesel engine using time resolved laser induced incandescence (TR-LII). *Combustion and Flame*, **159**, 2985–2998.

Menkiel, B., Donkerbroek, A., Uitz, R., Cracknell, R. and Ganippa, L. (2014). Combustion and soot processes of diesel and rapeseed methyl ester in an optical diesel engine. *Fuel*, **118**, 406–415.

Miles, P. C., Collin, R., Hildingsson, L., Hultqvist, A. and Andersson, Ö. (2007). Combined measurements of flow structure, partially oxidized fuel, and soot in a high-speed, direct-injection diesel engine. *Proc. Combustion Institute* **31**, **2**, 2963–2970.

Niessner, R. (2014). The many faces of soot: characterization of soot nanoparticles produced by engines. *Angewandte Chemie Int. Edition* **53**, **46**, 12366–12379.

Park, C., Lee, S. and Yi, U. (2016). Effects of engine operating conditions on particle emissions of lean-burn gasoline direct-injection engine. *Energy*, **115**, 1148–1155.

Pastor, J. V., García-Oliver, J. M., García, A., Micó, C. and Möller, S. (2016). Application of optical diagnostics to the quantification of soot in n-alkane flames under diesel conditions. *Combustion and Flame*, **164**, 212–223.

Rao, L., Zhang, Y., Kim, D., Su, H. C., Kook, S., Kim, K. S. and Kweon, C. B. (2018). Effect of after injections on late cycle soot oxidation in a small-bore diesel engine. *Combustion and Flame*, **191**, 513–526.

Seong, H., Lee, K. and Choi, S. (2013). Effects of engine operating parameters on morphology of particulates from a gasoline direct injection (GDI) engine. *SAE Technical Paper No.* 2013-01-2574.

Smallwood, G. J., Clavel, D., Gareau, D., Sawchuk, R. A., Snelling, D. R., Witze, P. O., Axelsson, B., Bachalo, W. D. and Gülder, Ö. L. (2002). Concurrent quantitative laser-induced incandescence and SMPS measurements of EGR

effects on particulate emissions from a TDI diesel engine. *SAE Trans*., 1345–1360.

Snelling, D. R., Smallwood, G. J., Liu, F., Gülder, Ö. L. and Bachalo, W. D. (2005). A calibration-independent laser-induced incandescence technique for soot measurement by detecting absolute light intensity. *Applied Optics* **44**, **31**, 6773–6785.

Stevens, E. and Steeper, R. (2001). Piston wetting in an optical DISI engine: fuel films, pool fires, and soot generation. *SAE Trans*., 1287–1294.

Stojkovic, B. D., Fansler, T. D., Drake, M. C. and Sick, V. (2005). High-speed imaging of OH^* and soot temperature and concentration in a stratified-charge direct-injection gasoline engine. *Proc. Combustion Institute*, **30**, 2657–2665.

Su, H. C., Kook, S., Chan, Q. N., Hawkes, E. R., Le, M. K. and Ikeda, Y. (2018). A comparison of high-temperature reaction and soot processes of conventional diesel and methyl decanoate. *Fuel*, **226**, 635–643.

Uy, D., Ford, M. A., Jayne, D. T., O'Neill, A. E., Haack, L. P., Hangas, J., Jagner, M. J., Sammut, A., Gangopadhyay, A. K. (2014). Characterization of gasoline soot and comparison to diesel soot: morphology, chemistry, and wear. *Tribology Int.*, **80**, 198–209.

Velji, A., Yeom, K., Wagner, U., Spicher, U., Roßbach, M., Suntz, R. and Bockhorn, H. (2010). Investigations of the formation and oxidation of soot inside a direct injection spark ignition engine using advanced laser-techniques. *SAE Technical Paper No*. 2010-01-0352.

Wang, Y., Makwana, A., Iyer, S., Linevsky, M., Santoro, R. J., Litzinger, T. A. and O'Connor, J. (2018). Effect of fuel composition on soot and aromatic species distributions in laminar, co-flow flames. Part 1. Non-premixed fuel. *Combustion and Flame*, **189**, 443–455.

Witkowski, D., Kondo, K., Vishwanathan, G. and Rothamer, D. (2013). Evaluation of the sooting properties of real fuels and their commonly used surrogates in a laminar co-flow diffusion flame. *Combustion and Flame*, **160**, 1129–1141.

Zhang, M., Hong, W., Xie, F., Su, Y., Han, L. and Wu, B. (2018a). Experimental investigation of impacts of injection timing and pressure on combustion and particulate matter emission in a spray-guided gdi engine. *Int. J. Automotive Technology* **19**, **3**, 393–404.

Zhang, M., Hong, W., Xie, F., Su, Y., Liu, H. and Zhou, S. T. (2018b). Combustion, performance and particulate matter emissions analysis of operating parameters on a GDI engine by traditional experimental investigation and Taguchi method. *Energy Conversion and Management*, **164**, 344–352.

Zhang, R., Pham, P. X., Kook, S. and Masri, A. R. (2019). Influence of biodiesel carbon chain length on in-cylinder soot processes in a small bore optical diesel engine. *Fuel*, **235**, 1184–1194.

Zheng, L., Ma, X., Wang, Z. and Wang, J. (2015). An optical study on liquid-phase penetration, flame lift-off location and soot volume fraction distribution of gasoline–diesel blends in a constant volume vessel. *Fuel*, **139**, 365–373.

Zimmerman, N., Wang, J. M., Jeong, C. H., Wallace, J. S. and Evans, G. J. (2016). Assessing the climate trade-offs of gasoline direct injection engines. *Environmental Science Technology* **50**, **15**, 8385–8392.